UC San Diego
UC San Diego Previously Published Works

Title

Role of Na+ Interstitials and Dopants in Enhancing the Na+ Conductivity of the Cubic Na3PS4 Superionic Conductor

Permalink

https://escholarship.org/uc/item/0rh6k0h8

Journal

Chemistry of Materials, 27(24)

ISSN

0897-4756

Authors

Zhu, Zhuoying
Chu, Iek-Heng
Deng, Zhi
et al.

Publication Date

2015-12-22

DOI

10.1021/acs.chemmater.5b03656

Peer reviewed

Role of Na$^+$ Interstitials and Dopants in Enhancing the Na$^+$ Conductivity of the Cubic Na$_3$PS$_4$ Superionic Conductor

Zhuoying Zhu, Iek-Heng Chu, Zhi Deng, and Shyue Ping Ong*

Department of NanoEngineering, University of California, San Diego, 9500 Gilman Drive, Mail Code 0448, La Jolla, California 92093, United States

S *Supporting Information*

ABSTRACT: In this work, we performed a first-principles investigation of the phase stability, dopant formation energy and Na$^+$ conductivity of pristine and doped cubic Na$_3$PS$_4$ (c-Na$_3$PS$_4$). We show that pristine c-Na$_3$PS$_4$ is an extremely poor Na ionic conductor, and the introduction of Na$^+$ excess is the key to achieving reasonable Na$^+$ conductivities. We studied the effect of aliovalent doping of M^{4+} for P^{5+} in c-Na$_3$PS$_4$, yielding Na$_{3+x}$M$_x$P$_{1-x}$S$_4$ (M = Si, Ge, and Sn with $x = 0.0625$; M = Si with $x = 0.125$). The formation energies in all the doped structures with dopant concentration of $x = 0.0625$ are found to be relatively low. Using *ab initio* molecular dynamics simulations, we predict that 6.25% Si-doped c-Na$_3$PS$_4$ has a Na$^+$ conductivity of 1.66 mS/cm, in excellent agreement with previous experimental results. Remarkably, we find that Sn^{4+} doping at the same concentration yields a much higher predicted Na$^+$ conductivity of 10.7 mS/cm, though with a higher dopant formation energy. A higher Si^{4+} doping concentration of $x = 0.125$ also yields a significant increase in Na$^+$ conductivity with an even higher dopant formation energy. Finally, topological and van Hove correlation function analyses suggest that the channel volume and correlation in Na$^+$ motions may play important roles in enhancing Na$^+$ conductivity in this structure.
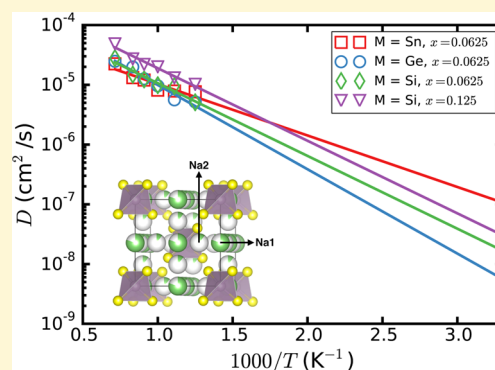
INTRODUCTION

Rechargeable Na-ion batteries have enjoyed a resurgence of interest in recent years,[1−4] propelled in part by concerns about the global availability of lithium, and also by the exciting possibility of novel chemistries. Though significant advances have been made in the development of Na-ion cathodes and anodes,[5−7] a major impediment to the commercial viability of rechargeable Na-ion batteries is the lack of an effective electrolyte. Current Na-ion electrolytes are mostly based on the same fundamental chemistry as Li-ion electrolytes, a mixture of cyclic and linear organic carbonates with a Na-salt.[8] Such organic solvent-based liquid electrolytes are flammable and have limited electrochemical windows.[9−12]

A promising alternative architecture is all-solid-state Na-ion battery utilizing nonflammable ceramic Na superionic conductor electrolytes. Na solid electrolytes such as β-alumina and NAtrium Superionic CONductors (NASICON) are well-studied, but they typically exhibit reasonable ionic conductivities only at higher temperatures.[7,13−16]

An exciting recent development is the discovery of the cubic phase of Na$_3$PS$_4$ (c-Na$_3$PS$_4$, space group: $I\bar{4}3m$) in 2012.[14] Initially reported to have a Na$^+$ conductivity of 0.2 mS/cm,[14] Hayashi and co-workers were able to subsequently enhance the conductivity of c-Na$_3$PS$_4$ to 0.46 mS/cm using crystalline Na$_2$S with high purity of over 99% followed by heat treatment.[17] Further efforts at optimizing the conductivity within the $(1 − x)$Na$_3$PS$_4$·xNa$_4$SiS$_4$ pseudobinary system yield a maximum

ionic conductivity as high as 0.74 mS/cm at x around 0.06.[18,19] Recent first-principles work also shows that Na$_3$PS$_4$ is likely to have favorable elastic properties that allow good electrode contact to be achieved with cold-press sintering.[20]

c-Na$_3$PS$_4$ is therefore a promising solid electrolyte candidate, particularly if its ionic conductivity is further improved with proper doping strategies. Using first-principles computational methods, one can rapidly investigate the microscopic mechanisms of diffusion in c-Na$_3$PS$_4$ and the effect of doping on its overall conductivity.[21,22] The insights gained from such an exercise would not only guide further optimization, but also provide important insights for design of other novel Na superionic conductors.

In this article, we performed a first-principles investigation of the phase stability and Na$^+$ ionic transport in undoped and M^{4+}-doped (M = Si, Ge, and Sn) c-Na$_3$PS$_4$. We demonstrate that pristine c-Na$_3$PS$_4$ is in fact an extremely poor ionic conductor, but with the introduction of Na$^+$ interstitials, a reasonably high conductivity can be achieved. We further demonstrate that 6.25% doping of Si^{4+} for P^{5+} with the concomitant introduction of compensating Na$^+$ interstitials result in Na$_{3+x}$Si$_x$P$_{1-x}$S$_4$ with predicted Na$^+$ conductivities that are in excellent agreement with previous experimental results.
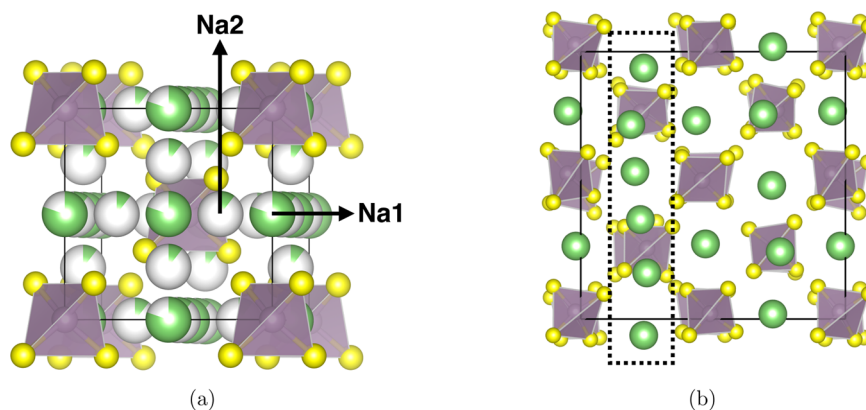
Figure 1. (a) Crystal structure of c-Na_3PS_4 primitive cell with green−white spheres, which represent the partially occupied Na sites, whereas dark purple tetrahedrons are PS_4^{3-}. (b) The lowest energy ordering of the 2 × 2 × 2 c-Na_3PS_4 supercell with an Na^+ interstitial (located within the dashed rectangle).

Furthermore, we show that increased Si^{4+} doping (from $x =$ 0.0625 to 0.125) and Sn^{4+} doping can potentially achieve even higher conductivities.

METHODS

All calculations were performed with the Vienna *Ab initio* Simulation Package (VASP),[23] within the projector augmented wave (PAW) approach.[24] The Perdew−Burke−Ernzerhof (PBE) generalized-gradient approximation (GGA)[25] was adopted for the exchange-correlation functional. Other parameters such as kinetic energy cutoff, k-mesh were carefully chosen under different situations to ensure the convergence of energies while keeping the computational cost reasonable, as detailed in the subsections below. The Python Materials Genomics (pymatgen) materials analysis library[26] was used for all analyses.

Phase Stability. Cubic Na_3PS_4 ($I\overline{4}3m$) has two symmetrically distinct Na sites: the 6 *b* site (Na1) with a partial occupancy of 0.8, and the 12 *d* site (Na2) with a partial occupancy of 0.1 (Figure 1a).[19] Structural optimizations were carried out on all symmetrically distinct orderings of the primitive cell enumerated using the algorithm of Hart et al.[27] We then selected the lowest energy configuration in subsequent calculations.

We also studied $Na_{3+x}M_xP_{1-x}S_4$ with M = Si, Ge, and Sn in this work. Since the maximum ionic conductivity reported by Hayashi et al.[18,19] was achieved with Si/P ratio equal to 6:94, an initial value of x = 0.0625 was chosen to mimic the reported dopant concentration. The doped systems were constructed using a 2 × 2 × 2 supercell of the conventional unit cell of c-Na_3PS_4, in which one P^{5+} is replaced by M^{4+} (Si, Ge, or Sn) and a Na^+ added to maintain overall charge neutrality. For M = Si, we also studied the effect of dopant concentration by doubling x to 0.125 with corresponding increase in Na^+ concentration.

The calculation parameters used (spin-polarized, kinetic energy cutoff of 520 eV and k-point density of 1000 per atom) are consistent with those used in the Materials Project (MP).[28] The phase stabilities of c-Na_3PS_4 and $Na_{3+x}M_xP_{1-x}S_4$ were investigated by constructing the Na−M−P−S phase diagrams[29] using precomputed energies of existing $Na_xP_yS_z$ and $Na_wM_xP_yS_z$ compounds in the MP database extracted via the Materials Application Programming Interface.[30] To ensure a good coverage of the Na−P−S chemical space, we also performed S for O substitution of all Na−P−O and Na for Li substitution of all Li−P−S compounds and included the $Na_4P_2S_6$ and $Na_2P_2S_6$ structures that were reported recently.[31,32]

For all materials of interest, we computed the decomposition energy (also known as the energy above hull), E_{decomp}, of each phase of interest to the most stable linear combination of equilibrium phases in the Na−P−S or Na−M−P−S phase diagram.[29] Stable phases would have an E_{decomp} of 0, while the higher the E_{decomp}, the more unstable a phase is.

Correction for Sulfur. In our investigations, we found that the binding energy of ground state sulfur (monoclinic S_8) is significantly overestimated by the PBE functional, similar to the well-known overbinding observed for the O_2 molecule.[33] Following a similar methodology as that proposed by Wang et al., we have fitted a correction for sulfur using the formation energies of main group sulfides (see Supporting Information). This correction, which corrects for both the overbinding as well as the incomplete self-interaction error cancellation in going from S_8 to S^{2-}, is estimated to be −0.66 eV per S atom and is applied to all subsequent analyses. This correction will be incorporated into the Materials Project to improve predicted sulfide formation energies.

Dopant Formation Energy. Neutral dopant formation energies were calculated using the formalism presented by Wei et al.[34]

$$E_f[M] = E_{tot}[M] - E_{tot}[bulk] - \sum_i n_i \mu_i \qquad (1)$$

where $E_{tot}[M]$ and $E_{tot}[bulk]$ are the total energies of the structure with and without the neutral dopant M, respectively; μ_i is the atomic chemical potential of species i that varies based on different experimental conditions; n_i indicates the number of atoms of species i being added ($n_i > 0$) or removed ($n_i < 0$) from the pristine structure. μ_i can be defined as $\mu_i = E_i + \Delta\mu_i$, where $\Delta\mu_i$ is the chemical potential of species i referenced to the elemental solid/gas with energy E_i. In the case of $Na_{3+x}M_xP_{1-x}S_4$ with M = Si, Ge, and Sn, and x = 0.0625, the formation of the defect structure involves an addition of the dopant M^{4+} and a Na^+ interstitial, together with the removal of a host P^{5+} ion. The corresponding formation energy E_f can be expressed as follows:

$$E_f[M] = E_f^0[M] - \Delta\mu_M - \Delta\mu_{Na} + \Delta\mu_P \qquad (2)$$

$$E_f^0[M] = E_{tot}[M] - E_{tot}[bulk] - E_M - E_{Na} + E_P \qquad (3)$$

Additional constraints can be applied to the atomic chemical potentials μ_i under equilibrium growth conditions. First, to avoid precipitation of the elemental M, Na, P, and S, $\Delta\mu_i \leq 0$. Second, to maintain a stable c-Na_3PS_4 framework structure during synthesis

$$E_f[Na_3PS_4] = 3\Delta\mu_{Na} + \Delta\mu_P + 4\Delta\mu_S \qquad (4)$$

where $E_f[Na_3PS_4]$ is the formation energy of the pristine c-Na_3PS_4 per formula unit (f.u.). Third, possible secondary phases formed between the dopant M and the framework structure are to be avoided as well. In the case of $Na_{3+x}Si_xP_{1-x}S_4$ with x = 0.0625, for example, the formation of the possible secondary phase Na_4SiS_4, as indicated in Table 1, should be avoided. This leads to the following inequality:

$$4\Delta\mu_{Na} + \Delta\mu_{Si} + 4\Delta\mu_S \leq E_f[Na_4SiS_4] \qquad (5)$$

where $E_f[Na_4SiS_4]$ is the formation energy of Na_4SiS_4.

Table 1. Decomposition Energies E_{decomp}, the Corresponding Decomposed Products, and Neutral Dopant Formation Energies E_f of the Doped c-Na_3PS_4 Compared with Undoped Case

dopant M	x	E_f (eV/f.u.)	E_{decomp} (meV/atom)	decomposed products
undoped	N/A	N/A	5	t-Na_3PS_4
Si	0.125	1.65	30	t-Na_3PS_4, Na_4SiS_4
Si	0.0625	1.04	13	t-Na_3PS_4, Na_4SiS_4
Ge	0.0625	1.04	13	t-Na_3PS_4, $Na_6Ge_2S_7$, Na_2S
Sn	0.0625	1.32	15	t-Na_3PS_4, Na_4SnS_4

The lower bound of the dopant formation energy can be directly estimated using the above formalism and is equal to $E_{\text{decomp}}[\text{M}] - E_{\text{decomp}}[\text{bulk}]$ where $E_{\text{decomp}}[\text{M}]$ and $E_{\text{decomp}}[\text{bulk}]$ are, respectively, the decomposition energies of the M-doped and pristine c-Na_3PS_4.[35,36] Unless mentioned explicitly, the calculated dopant energies presented in the next section refer to this lower bound.

***Ab Initio* Molecular Dynamics Simulations.** The diffusivities and conductivities of the pristine and doped c-Na_3PS_4 structures were calculated using *ab initio* molecular dynamics (AIMD) simulations. Apart from the aforementioned doped structures, defect structure where a single Na^+ excess is introduced was also studied by removing an electron with a compensating background charge. In all simulations, the lowest energy configurations with a unit cell size equivalent to that of the $2 \times 2 \times 2$ c-Na_3PS_4 were selected.

Similar AIMD simulation parameters were used as per previous work by the authors.[21,37] Nonspin-polarized AIMD simulations were conducted in the NVT ensemble at 800−1400 K with a Nose−Hoover thermostat.[38,39] A smaller plane-wave energy cutoff of 280 eV and a minimal Γ-centered $1 \times 1 \times 1$ k-point mesh were adopted. The time step of the simulations was 2 fs. The initial structure was fully relaxed at 0 K, and the volume was fixed for AIMD simulations at elevated temperatures until the diffusivity is converged. No framework melting was observed in all simulations. All calculations were automated using an in-house AIMD workflow.[40,41] The central quantity obtained from each AIMD simulation is the Na ion diffusivity that can be expressed as

$$D = \frac{1}{2dt}\langle[\Delta\mathbf{r}(t)]^2\rangle \tag{6}$$

where d is the dimensionality factor and equals 3 for 3-D crystal structures, and $\langle[\Delta\mathbf{r}(t)]^2\rangle$ is the average mean square displacement (MSD) over a time duration t.

The diffusivity was obtained by performing a linear fitting of the MSD vs $2dt$. The Arrhenius plots were constructed to determine the activation energies and obtain extrapolated room-temperature diffusivities D_{300K}. The room-temperature Na ion conductivity σ_{300K} can then be derived from the Nernst−Einstein equation as follows:

$$\sigma_{300K} = \frac{\rho z^2 F^2}{RT}D_{300K} \tag{7}$$

where ρ is the molar density of diffusing Na ions in the unit cell; $z = +1$ is the charge of Na ions; and F and R are the Faraday's constant and the gas constant, respectively. $T = 300$ K was used in the above equation. It should be noted that the Nernst−Einstein relation applies only for uncorrelated species diffusion. The implication of correlated motion will be discussed in the Discussion section.

van Hove Correlation Function Analysis. To investigate the correlations in the Na ionic motions, we calculated and plotted the van Hove correlation function using trajectories from our AIMD simulations, which can be split into the self-part G_s and the distinct-part G_d as follows:

$$G_s(r, t) = \frac{1}{4\pi r^2 N_d}\langle\sum_{i=1}^{N_d} \delta(r - |\mathbf{r}_i(t_0) - \mathbf{r}_i(t + t_0)|)\rangle_{t_0} \tag{8}$$

$$G_d(r, t) = \frac{1}{4\pi r^2 \rho N_d}\langle\sum_{i\neq j}^{N_d} \delta(r - |\mathbf{r}_i(t_0) - \mathbf{r}_j(t + t_0)|)\rangle_{t_0} \tag{9}$$

Here, $\delta(\cdot)$ is the one-dimensional Dirac delta function. The angular bracket stands for the ensemble average over the initial time t_0. $\mathbf{r}_i(t)$ denotes the position of the ith particle at time t. N_d and r are the number of diffusing Na ions in the unit cell and radial distance, respectively. The presence of the average number density ρ serves as the "normalization factor" in G_d such that $G_d \rightarrow 1$ when $r \gg 1$. For a given r and t, $G_s(r, t)$ describes how probable a particle diffuses away from its initial position by a distance of r after time t, whereas $G_d(r, t)$ describes the radial distribution of $N - 1$ particles after time t with respect to the initial reference particle. In particular, $G_d(r, t)$ is reduced to the static pair distribution function when $t = 0$.

■ RESULTS

Phase Stability Analysis. c-Na_3PS_4 belongs to the $I\bar{4}3m$ space group with a lattice parameter of 6.9965(9) Å.[19] It is the high-temperature phase of the tetragonal Na_3PS_4 (t-Na_3PS_4). The lattice parameters for t- and c-Na_3PS_4 differ only by around 0.1 Å, and the experimental transition temperature from t-Na_3PS_4 to c-Na_3PS_4 is around 540 K.[14,42] The major difference is that the tetragonal phase is an ordered structure, whereas the cubic phase is disordered with two distinct sodium sites.

The E_{decomp} and the corresponding equilibrium phases for the undoped and doped c-Na_3PS_4 phases are listed in Table 1. For the undoped c-Na_3PS_4, our calculation predicts its E_{decomp} to be only 5 meV/atom, with t-Na_3PS_4 being the stable phase. This result is consistent with previous experimental data that the cubic phase is the metastable phase that is likely entropically stabilized.[14] With the introduction of a Na^+ interstitial, we find that the Na sites redistribute to maintain an approximately even distribution within a chain, leading to Na atoms that are slightly displaced from the Na1 and Na2 positions (Figure 1b).

Our results show that at $x = 0.0625$, the E_{decomp} of the M^{4+}-doped structures are 13 meV/atom for M = Si and Ge, and 15 meV/atom for Sn, respectively. The relatively low decomposition energies indicate that though these doped structures are metastable at 0 K, they can potentially be stabilized at room temperature by entropic effects. This is in qualitative agreement with the synthesizibility of Si-doped Na_3PS_4 with similar dopant concentration in experiments.[18] At a higher Si dopant concentration with $x = 0.125$, the resulting E_{decomp} increases to 30 meV/atom, indicating that the structure is more unstable. For Si, Sn-doped structures, the predicted equilibrium phases are t-Na_3PS_4 and Na_4MS_4 (M = Si, Sn), while the Ge-doped structure has the equilibrium phases of $Na_6Ge_2S_7$, Na_2S, and t-Na_3PS_4. Note that the sulfur energy correction does not affect the decomposition products in the systems studied in this work. This is because the t-Na_3PS_4 and Na_4SiS_4 remain stable before and after the sulfide correction.

Dopant Formation Energies. The dopant formation energy is an important quantity that measures the synthesizibility of the materials with dopants. The dopant formation energies of all dopants studied are tabulated in Table 1. At $x = 0.0625$, we find relatively low doping energies of 1.04 eV for both 6.25% Ge and Si doping compared to 6.25% Sn doping (1.32 eV) or 12.5% Si doping (1.65 eV). We note that Si doping in c-Na_3PS_4 was experimentally achieved for x up to 0.1. Since the dopant formation energy of 6.25% Sn lies between the dopant formation energies of 6.25% and 12.5% Si doping, we expect that 6.25% Sn-doping of c-Na_3PS_4 to be achievable experimentally.
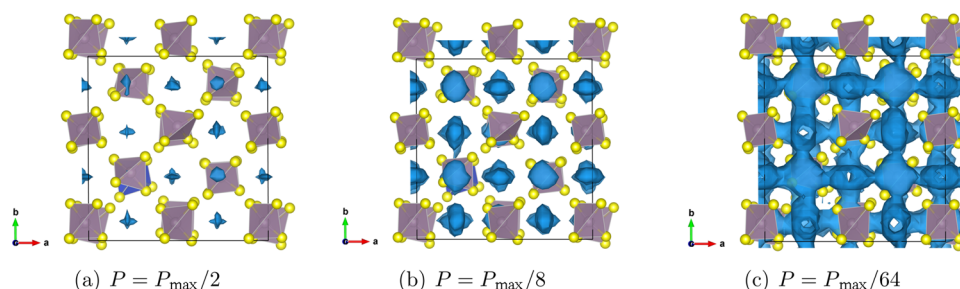
(a) $P = P_{max}/2$ (b) $P = P_{max}/8$ (c) $P = P_{max}/64$

Figure 2. Isosurfaces (blue) of Na ion probability density distribution P for $Na_{3+x}Si_xP_{1-x}S_4$ ($x = 0.0625$) at 800 K.

Probability Density and Site Occupancy. The probability density distribution defined on a uniform 3-D grid, namely, $P(\mathbf{r})$, is a powerful tool for investigating the ion diffusion of a given species. Two important pieces of information can be obtained from the distribution: (1) high probability sites where the ions tend to reside, which correspond to the low-energy sites in the structure, (2) the pathways of the ions among the low-energy sites.[43] In this work, P is obtained by first counting the number of Na ions at each point in the spatial uniform grid within a given time scale. A time averaging is then performed for P. Also, P is normalized such that $\int_\Omega P d\mathbf{r} = 1$ with Ω being the volume of the unit cell. We define the maximum of $P(\mathbf{r})$ as P_{max}.

Figure 2 shows the isosurfaces of probability density distributions for Na ions in $Na_{3+x}Si_xP_{1-x}S_4$ ($x = 0.0625$) at 800 K (the lowest temperature at which the AIMD simulations were performed) at various cutoffs. In general, the $P(\mathbf{r})$ are fairly similar across all systems investigated. As expected, we find that the high probability density positions correspond to the high occupancy (low energy) Na1 sites. As the cutoff is decreased, the isosurfaces show that the Na1 sites are connected to one another via the lower occupancy Na2 sites. We may therefore surmise that the Na2 sites are local minima sites with non-negligible occupation probability that help mediate Na^+ transport in this structure.

We also calculated the average site occupancies of the different Na sites at 800 K. The site occupancies for the Na1 and Na2 sites for the $Na_{3+x}Si_xP_{1-x}S_4$ ($x = 0.0625$) are 0.76 and 0.13, respectively, which are fairly close to the reported site occupancies of 0.8 and 0.11, respectively.[19] The deviations between the calculated occupancies and experiments are likely due to the fact that the AIMD simulations are carried out at higher temperatures (800 K) compared to experiments (300 K). Similar trends are observed for Ge-doped, Sn-doped, and Na-excess c-Na_3PS_4 (see Table S1 in Supporting Information). For the pristine c-Na_3PS_4, the average site occupancy for Na2 is less than 0.1 even at 800 K.

Na^+ Conductivity. Figure 3 shows the Arrhenius plots of the log of the diffusivity, D, versus the reciprocal of the temperature, $1000/T$, for the systems of interest. Diffusivities at six temperatures (800, 900, 1000, 1100, 1200, and 1400 K) are plotted for all systems except for pristine c-Na_3PS_4 where simulations at only four temperatures were run. Table 2 summarizes the extrapolated diffusivities D_{300K} and ionic conductivities σ_{300K}, including the error range for σ_{300K}.

From Figure 3a, we may observe that the calculated Na^+ conductivity is extremely low (1.1×10^{-4} mS/cm) and the activation barrier is extremely high (537 meV) in the pristine c-Na_3PS_4 material. The introduction of a Na^+ interstitial increases
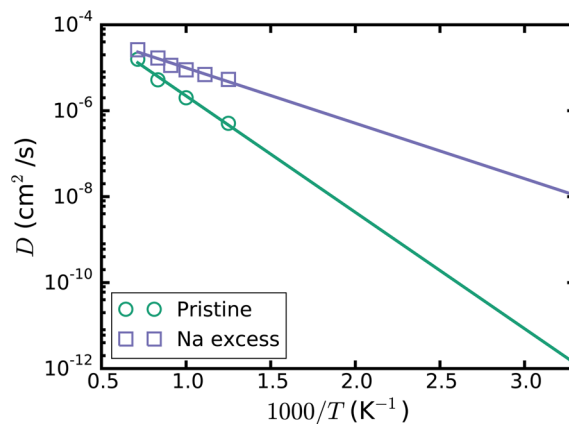

(a)
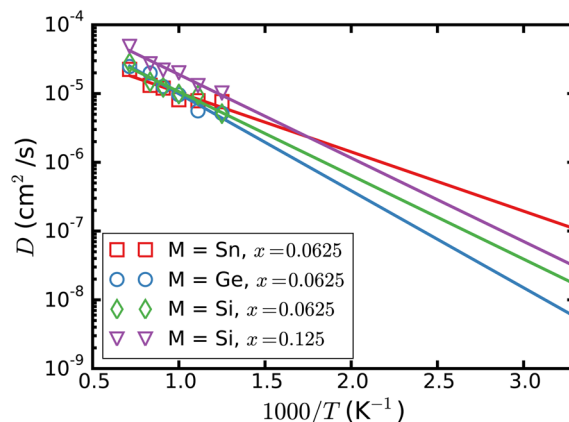
(b)

Figure 3. Arrhenius plots for (a) c-Na_3PS_4 with Na^+ excess and pristine structures; (b) doped structures $Na_{3+x}M_xP_{1-x}S_4$ (M = Si, Ge, or Sn).

the conductivity by 4 orders of magnitude to 1.06 mS/cm, while the activation energy decreases to 256 meV.

In practical materials, aliovalent doping is a common approach to modifying the Na concentration. In c-Na_3PS_4, Na^+ interstitials can be created by doping the P^{5+} sites with M^{4+} cations such as Sn^{4+}, Ge^{4+}, and Si^{4+}. The Arrhenius plots for doped $Na_{3+x}M_xP_{1-x}S_4$ with different values of M and x are given in Figure 3b, and the corresponding room-temperature conductivities and activation energies are reported in Table 2 as well. In general, we observe that similar Na^+ concentrations tend to result in similar conductivities (e.g., for $x = 0.0625$ in the Na-excess, Si-doped, and Ge-doped cases), indicating that this is the dominant factor influencing the overall ionic conductivity. The predicted room-temperature Na^+ conductiv-

Table 2. Channel Size, Channel Volume, Extrapolated Na^+ Conductivity, Diffusivity at 300 K, and Activation Energy

	x	channel size (Å)	channel volume (Å³)	σ_{300K} (mS/cm)	error range of σ_{300K} (mS/cm)	D_{300K} (cm²/s)	E_a (meV)
pristine	N/A	2.15	863	1.1×10^{-4}	$0.68–1.9 \times 10^{-4}$	1.1×10^{-12}	537
Na^+ excess	0.0625	2.15	874	1.06	0.79–1.40	9.8×10^{-9}	256
$Na_{3+x}Si_xP_{1-x}S_4$	0.125	2.16	879	2.99	2.27–3.94	2.8×10^{-8}	241
$Na_{3+x}Si_xP_{1-x}S_4$	0.0625	2.13	869	1.66	1.14–2.41	1.5×10^{-8}	242
$Na_{3+x}Ge_xP_{1-x}S_4$	0.0625	2.16	873	0.54	0.38–0.78	5.1×10^{-9}	280
$Na_{3+x}Sn_xP_{1-x}S_4$	0.0625	2.16	910	10.7	6.86–16.8	1.0×10^{-7}	171

(a) M=Si, $x = 0.0625$

(b) M=Ge, $x = 0.0625$

(c) M=Sn, $x = 0.0625$

(d) M=Si, $x = 0.125$
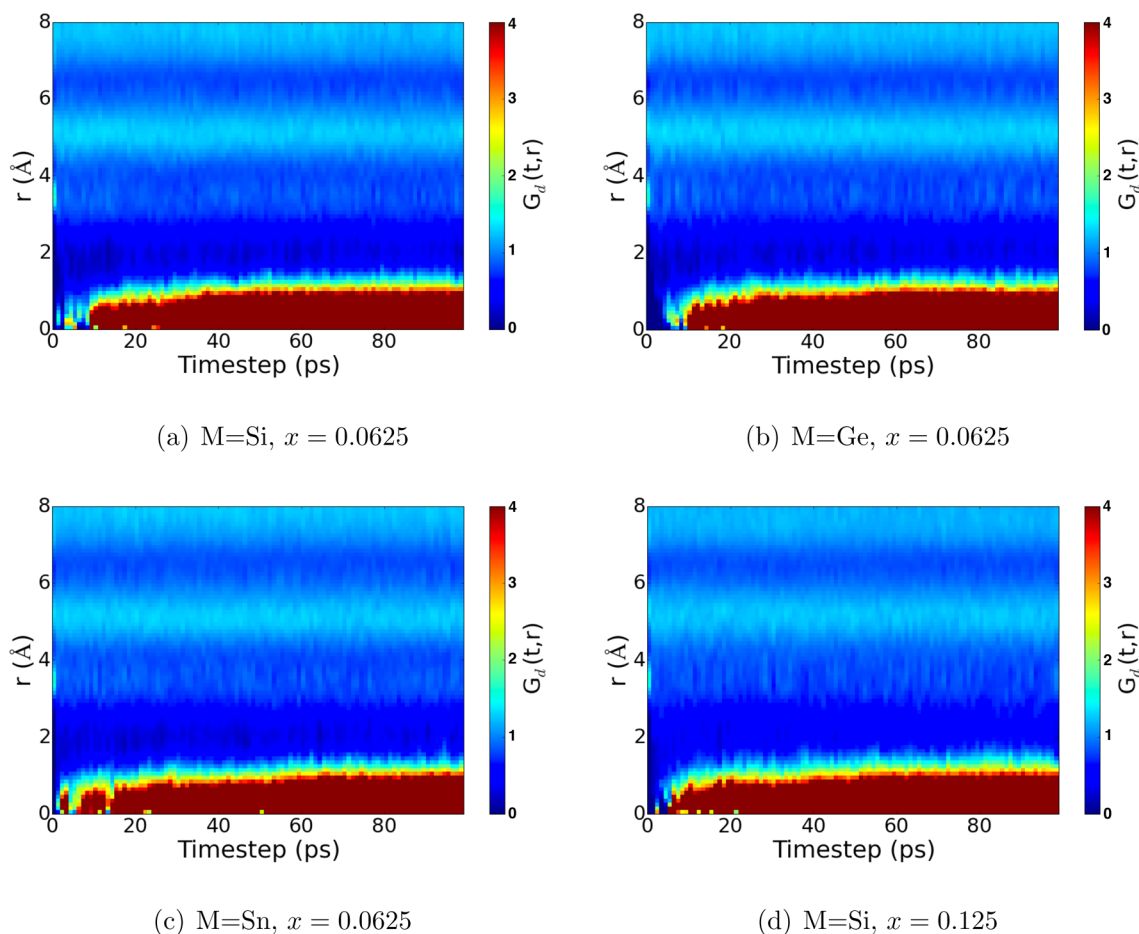
Figure 4. Plots of the distinct-part of the van Hove correlation function (G_d) for $Na_{3+x}M_xP_{1-x}S_4$ at 800 K. G_d is a function of the Na−Na pair distance r and time t.

ity for $Na_{3.0625}Si_{0.0625}P_{0.9375}S_4$ is 1.66 mS/cm, in excellent agreement with the previously measured experimental value of 0.74 mS/cm for $0.94Na_3PS_4 \cdot 0.06Na_4SiS_4$.[18,19]

Remarkably, the Sn-doped c-Na_3PS_4 is predicted to have a significantly higher Na^+ conductivity of 10.7 mS/cm compared to the other doped structures. The activation energy for diffusion in this material is also the smallest at 171 meV. We also investigated the effect of different dopant concentrations in the case of the Si-doped structure. From Figure 3b and Table 2, we may observe that higher doping concentrations can potentially enhance the Na^+ conductivity further to 2.99 mS/cm, though at the cost of increased dopant formation energy and decreased phase stability (see Table 1).

Channel Size, Channel Volume, and van Hove Function. Using the open source Zeo++ software,[44,45] we performed a topological analysis of all systems of interest. In all these materials, Na ions were removed from the relaxed structures to compute the largest radius of the free sphere that can pass through the remaining structure formed by framework cations and anions (P^{5+}, S^{2-}, and M^{4+}), which is defined as "channel size" and shown in Table 2. In general, the channel sizes for all cases are very similar to the difference of no more than 0.03 Å. At a dopant concentration of $x = 6.25\%$, both Ge- and Sn-doped structures have the largest channel sizes.

Using the ionic trajectories from AIMD simulations at 800 K, we also calculated the average channel volumes of all systems investigated. This quantity is defined as the unit cell volume minus the volume of the framework polyhedrons (PS_4 or MS_4), and it describes the "free volume" for Na ions during the diffusion. The results are given in Table 2. We find that the channel volumes in all doped structures are very similar to each other, with the exception of Sn-doped structure where the channel volume is more than 4% higher than those in the rest of the cases.

Figure 4 presents the distinct part of the van Hove correlation function G_d for each doped-structure at 800 K.

Our calculations show that G_d of all the doped structures always exhibit a pronounced peak at the proximity of $r = 0$, indicating that the Na ion motions in these materials are highly correlated. The correlated motion in the Sn^{4+} doped structure (Figure 4c) takes place sooner than the other doped structures with the same dopant concentration. This is in accordance with the higher diffusion coefficient found in this structure. In fact, we observe a large amount of single Na^+ hops between neighboring Na1 and Na2 sites within a 1 ps time scale as well as correlated hops between adjacent Na ions in our AIMD trajectories.

■ DISCUSSION

c-Na_3PS_4 is a highly promising sodium superionic conductor whose ionic conductivity can be further enhanced by aliovalent doping. In this work, we conducted a comprehensive investigation of the phase stability, dopant formation energies, and Na^+ conductivities of pristine and doped c-Na_3PS_4, with the aim of understanding the reasons for its high conductivity and elucidating potential strategies to further push its conductivity beyond 1 mS/cm.

Our work shows that Na disorder induced by Na excess is key to the high ionic conductivity in c-Na_3PS_4. We find that stoichiometric c-Na_3PS_4 has a very low ionic conductivity, which is similar to reported value of t-Na_3PS_4.[42] Stoichiometric c-Na_3PS_4 also has relatively low occupancy on the Na2 site (<0.1 at 800 K), similar to t-Na_3PS_4. Both these observations are not surprising, given the small differences in lattice parameters between t- and c-Na_3PS_4. It is only when the Na^+ interstitials are introduced to c-Na_3PS_4 that the Na2 site occupancy increases and the Na^+ conductivity increases appreciably to the 0.1−1 mS/cm levels observed experimentally.

With these results in mind, it is therefore somewhat surprising that the initially reported ionic conductivity of pristine c-Na_3PS_4 by Hayashi et al. is as high as 0.2 mS/cm.[14] We speculate that there may have been doped impurities in the original sample, e.g., from the carbon electrodes or Zr, resulting in Na excess. It should be noted that Hayashi et al. specifically excluded Zr as a possible contaminant, and the calculated dopant formation energy of 6.25% Zr doping is estimated to be 1.45 eV/f.u., substantially higher than that for 6.25% Si doping (1.04 eV/f.u.). The fact that the same authors were subsequently able to obtain a significant increase in conductivity to 0.46 mS/cm using a Na_2S precursor with high purity[17] further supports the hypothesis that Na^+ interstitial defects are crucial to achieving high Na^+ conductivity in this structure. Though a purer Na_2S does not necessarily mean Na^+ interstitials will be formed, a less pure Na_2S precursor can potentially result in Na deficiency and reduce the likelihood of forming Na^+ interstitials.

The increase in conductivity with the introduction of Na^+ interstitials is likely caused by the increased Coulombic repulsion between Na^+, leading to a redistribution that causes Na to be slightly displaced from the Na1 and Na2 positions. We speculate that this redistribution leads to a shallow energy landscape that promotes the cooperative motion of Na, leading to lower activation barriers and increased conductivity. The van Hove correlation function analysis, which indicates that correlated Na motion happens within a relatively short time scale, supports this hypothesis. Indeed, the higher the conductivity (e.g., in Sn-doped c-Na_3PS_4), the shorter the time scale in which correlated motion occurs.

A typical strategy to introduce Na^+ interstitials is through aliovalent substitution of M^{4+} for P^{5+} in c-Na_3PS_4. At a Si doping concentration of 6.25%, the predicted room-temperature Na^+ conductivity of 1.66 mS/cm is in excellent agreement with the reported experimental conductivity of 0.74 mS/cm for $0.94Na_3PS_4·0.06Na_4SiS_4$ reported by Tanibata et al.[18,19] At a higher Si doping concentration of 12.5%, the predicted Na^+ conductivity further increases to 2.99 mS/cm, but the dopant formation energy increases substantially. This increased dopant formation energy is a possible reason why Tanibata et al. reported "unknown secondary phases" at doping concentrations beyond 10%.[18,19]

Among the M^{4+} dopants investigated, our calculations indicate that a particularly promising candidate for further investigation is Sn-doped structure. $Na_{3.0625}Sn_{0.0625}P_{0.9375}S_4$ is predicted to have a much higher Na^+ conductivity of 10.7 mS/cm, while the dopant formation energy is only slightly higher than Si doping at a similar concentration. Given that Si doping in c-Na_3PS_4 as high as 10% have been achieved experimentally, 6.25% Sn doping should be achievable. As of now, we can only speculate on the reasons why there is such a significant difference in conductivity between Sn versus Si doping. Topological analyses find that the Sn-doped structure has a slightly larger channel size and free channel volume for Na^+ diffusion than the Si-doped structure. However, a similar relative difference in channel size and volume in the $Li_{10}MP_2S_{12}$ (M = Si, Ge, and Sn) superionic conductor[26] leads to the opposite trend in Na^+ conductivity of Si > Sn. It may be that such different trends are the result of (a) the different dimensionality of diffusion in $Li_{10}MP_2S_{12}$ systems (quasi 1D) and doped Na_3PS_4 systems (3D), and (b) the different diffusing species, i.e., Li^+ in $Li_{10}MP_2S_{12}$ and Na^+ in c-Na_3PS_4. It is our hope that future experiments will verify if the Sn-doped structure can be synthesized, and if it does indeed exhibit higher conductivities than the Si and Ge-doped structures.

It should be noted that eq 6 provides a good estimate of the diffusivity only in the case of uncorrelated diffusion. The degree to which ionic motion is correlated is frequently described using the Haven ratio, H_R, which is defined as the ratio of the tracer diffusivity to the charge or dc diffusivity.[46,47] We have not attempted to determine this ratio from AIMD due to the extremely slow convergence of the charge diffusivity. Nevertheless, typical H_R values for similar highly correlated diffusion systems are in the range of 0.3−0.6 (e.g., $H_R[Li_{10}SnP_2S_{12}] \approx 0.3$).[48] We therefore expect that the computed diffusivities and conductivities in this work to be lower bound estimates that are off by no more than a factor of 3 and that the qualitative trends should remain valid.

■ CONCLUSIONS

To conclude, we have performed a comprehensive investigation of the phase stability, dopant formation energy, and Na^+ conductivity of c-Na_3PS_4 and $Na_{3+x}M_xP_{1−x}S_4$ (M = Si with x = 0.0625 and 0.125; M = Ge, Sn with x = 0.0625). Our results show that Na disorder induced by Na^+ excess is a key factor to enhancing the Na^+ conductivity in c-Na_3PS_4. Si^{4+}, Ge^{4+}, and Sn^{4+} are all viable dopants to introduce Na^+ excess in c-Na_3PS_4 for this purpose due to their relatively low dopant formation energies. Our calculated Na^+ conductivity of 1.66 mS/cm for 6.25% Si-doped c-Na_3PS_4 is in an excellent agreement with experiments. We also find that the Na^+ conductivity can be further enhanced by increasing Si dopant concentration from 6.25% to 12.5%, but at the cost of much higher dopant

formation energy. Finally, we predict that 6.25% Sn-doped c-Na_3PS_4 is a potentially promising Na superionic conductor with a significantly higher Na^+ conductivity than 6.25% Si-doped c-Na_3PS_4.

■ ASSOCIATED CONTENT

Ⓢ Supporting Information

The Supporting Information is available free of charge on the ACS Publications website at DOI: 10.1021/acs.chemmater.5b03656.

> Average Na1, Na2 site occupancies of all systems in this work, determination of sulfur correction, and the self-part of the van Hove correlation function for M-doped c-Na_3PS_4 (M = Si, Ge, Sn) (PDF)

■ AUTHOR INFORMATION

Corresponding Author
*E-mail: ongsp@eng.ucsd.edu.

Notes

The authors declare no competing financial interest.

■ ACKNOWLEDGMENTS

■ REFERENCES

(1) Larcher, D.; Tarascon, J.-M. Towards Greener and More Sustainable Batteries for Electrical Energy Storage. *Nat. Chem.* **2015**, *7*, 19−29.

(2) Hueso, K. B.; Armand, M.; Rojo, T. High Temperature Sodium Batteries: Status, Challenges and Future Trends. *Energy Environ. Sci.* **2013**, *6*, 734−749.

(3) Ellis, B. L.; Nazar, L. F. Sodium and Sodium-ion Energy Storage Batteries. *Curr. Opin. Solid State Mater. Sci.* **2012**, *16*, 168−177.

(4) Ong, S. P.; Chevrier, V. L.; Hautier, G.; Jain, A.; Moore, C.; Kim, S.; Ma, X.; Ceder, G. Voltage, Stability and Diffusion Barrier Differences Between Sodium-ion and Lithium-ion Intercalation Materials. *Energy Environ. Sci.* **2011**, *4*, 3680.

(5) Yabuuchi, N.; Kubota, K.; Dahbi, M.; Komaba, S. Research Development on Sodium-Ion Batteries. *Chem. Rev.* **2014**, *114*, 11636−11682.

(6) Li, X.; Ma, X.; Su, D.; Liu, L.; Chisnell, R.; Ong, S. P.; Chen, H.; Toumar, A.; Idrobo, J.-c.; Lei, Y.; Bai, J.; Wang, F.; Lynn, J. W.; Lee, Y. S.; Ceder, G. Direct Visualization of the Jahn-Teller Effect Coupled to Na Ordering in $Na_{5/8}MnO_2$. *Nat. Mater.* **2014**, *13*, 586−592.

(7) Pan, H.; Hu, Y.-S.; Chen, L. Room-temperature Stationary Sodium-ion Batteries for Large-scale Electric Energy Storage. *Energy Environ. Sci.* **2013**, *6*, 2338.

(8) Ponrouch, A.; Marchante, E.; Courty, M.; Tarascon, J.-M.; Palacín, M. R. In Search of An Optimized Electrolyte for Na-ion Batteries. *Energy Environ. Sci.* **2012**, *5*, 8572.

(9) Tarascon, J.-M.; Armand, M. Issues and Challenges Facing Rechargeable Lithium Batteries. *Nature* **2001**, *414*, 359−367.

(10) Xu, K. Electrolytes and Interphases in Li-Ion Batteries and Beyond. *Chem. Rev.* **2014**, *114*, 11503−11618.

(11) Armand, M.; Tarascon, J.-M. Building Better Batteries. *Nature* **2008**, *451*, 652−657.

(12) Xu, K. Nonaqueous Liquid Electrolytes for Lithium-based Rechargeable Batteries. *Chem. Rev.* **2004**, *104*, 4303−4417.

(13) Tatsumisago, M.; Hayashi, A. Sulfide Glass-Ceramic Electrolytes for All-Solid-State Lithium and Sodium Batteries. *Int. J. Appl. Glass Sci.* **2014**, *10*, 226−235.

(14) Hayashi, A.; Noi, K.; Sakuda, A.; Tatsumisago, M. Superionic Glass-Ceramic Electrolytes for Room-temperature Rechargeable Sodium Batteries. *Nat. Commun.* **2012**, *3*, 856.

(15) Anantharamulu, N.; Koteswara Rao, K.; Rambabu, G.; Vijaya Kumar, B.; Radha, V.; Vithal, M. A Wide-ranging Review on Nasicon Type Materials. *J. Mater. Sci.* **2011**, *46*, 2821−2837.

(16) Hooper, A. A Study of the Electrical Properties of Single-crystal and Polycrystalline β-alumina Using Complex Plane Analysis. *J. Phys. D: Appl. Phys.* **1977**, *10*, 1487−1496.

(17) Hayashi, A.; Noi, K.; Tanibata, N.; Nagao, M.; Tatsumisago, M. High Sodium Ion Conductivity of Glass-Ceramic Electrolytes with Cubic Na_3PS_4. *J. Power Sources* **2014**, *258*, 420−423.

(18) Tanibata, N.; Noi, K.; Hayashi, A.; Tatsumisago, M. Preparation and Characterization of Highly Sodium Ion Conducting Na_3PS_4·Na_4SiS_4 Solid Electrolytes. *RSC Adv.* **2014**, *4*, 17120−17123.

(19) Tanibata, N.; Noi, K.; Hayashi, A.; Kitamura, N.; Idemoto, Y.; Tatsumisago, M. X-ray Crystal Structure Analysis of Sodium-Ion Conductivity in $94Na_3PS_4$·$6Na_4SiS_4$ Glass-Ceramic Electrolytes. *ChemElectroChem* **2014**, *1*, 1130−1132.

(20) Deng, Z.; Wang, Z.; Chu, I.-H.; Luo, J.; Ong, S. P. Elastic Properties of Alkali Superionic Conductor Electrolytes from First Principles Calculations. *J. Electrochem. Soc.* **2016**, *163*, A67−A74.

(21) Ong, S. P.; Mo, Y.; Richards, W. D.; Miara, L.; Lee, H. S.; Ceder, G. Phase Stability, Electrochemical Stability and Ionic Conductivity of the $Li_{10±1}MP_2X_{12}$ (M = Ge, Si, Sn, Al or P, and X = O, S or Se) Family of Superionic Conductors. *Energy Environ. Sci.* **2013**, *6*, 148−156.

(22) Miara, L. J.; Ong, S. P.; Mo, Y.; Richards, W. D.; Park, Y.; Lee, J.-m.; Lee, H. S.; Ceder, G. Effect of Rb and Ta Doping on the Ionic Conductivity and Stability of the Garnet $Li_{7+2x-y}(La_{3-x}Rb_x)(Zr_{2-y}Ta_y)O_{12}$. *Chem. Mater.* **2013**, *25*, 3048−3055.

(23) Kresse, G. Efficient Iterative Schemes for Ab Initio Total-energy Calculations Using a Plane-wave Basis Set. *Phys. Rev. B: Condens. Matter Mater. Phys.* **1996**, *54*, 11169−11186.

(24) Blöchl, P. E. Projector Augmented-wave Method. *Phys. Rev. B: Condens. Matter Mater. Phys.* **1994**, *50*, 17953−17979.

(25) Perdew, J. P.; Burke, K.; Ernzerhof, M. Generalized Gradient Approximation Made Simple. *Phys. Rev. Lett.* **1996**, *77*, 3865−3868.

(26) Ong, S. P.; Richards, W. D.; Jain, A.; Hautier, G.; Kocher, M.; Cholia, S.; Gunter, D.; Chevrier, V. L.; Persson, K. a.; Ceder, G. Python Materials Genomics (Pymatgen): A Robust, Open-source Python Library for Materials Analysis. *Comput. Mater. Sci.* **2013**, *68*, 314−319.

(27) Hart, G. L. W.; Forcade, R. W. Algorithm for Generating Derivative Structures. *Phys. Rev. B: Condens. Matter Mater. Phys.* **2008**, *77*, 224115.

(28) Jain, A.; Ong, S. P.; Hautier, G.; Chen, W.; Richards, W. D.; Dacek, S.; Cholia, S.; Gunter, D.; Skinner, D.; Ceder, G.; Persson, K. A. Commentary: The Materials Project: A Materials Genome Approach to Accelerating Materials Innovation. *APL Mater.* **2013**, *1*, 011002.

(29) Ong, S. P.; Wang, L.; Kang, B.; Ceder, G. Li-Fe-P-O_2 Phase Diagram from First Principles Calculations. *Chem. Mater.* **2008**, *20*, 1798−1807.

(30) Ong, S. P.; Cholia, S.; Jain, A.; Brafman, M.; Gunter, D.; Ceder, G.; Persson, K. a. The Materials Application Programming Interface (API): A Simple, Flexible and Efficient API for Materials Data Based on REpresentational State Transfer (REST) Principles. *Comput. Mater. Sci.* **2015**, *97*, 209−215.

(31) Bergerhoff, G.; Hundt, R.; Sievers, R.; Brown, I. D. The Inorganic Crystal Structure Data Base. *J. Chem. Inf. Model.* **1983**, *23*, 66−69.

(32) Kuhn, A.; Eger, R.; Nuss, J.; Lotsch, B. V. Synthesis and Structural Characterization of the Alkali Thiophosphates $Na_2P_2S_6$, $Na_4P_2S_6$, $K_4P_2S_6$ and $Rb_4P_2S_6$. *Z. Anorg. Allg. Chem.* **2014**, *640*, 689−692.

(33) Wang, L.; Maxisch, T.; Ceder, G. Oxidation Energies of Transition Metal Oxides within the GGA+U Framework. *Phys. Rev. B: Condens. Matter Mater. Phys.* **2006**, *73*, 195107.

(34) Wei, S.-H.; Zhang, S. Chemical Trends of Defect Formation and Doping Limit in II-VI Semiconductors: The Case of CdTe. *Phys. Rev. B: Condens. Matter Mater. Phys.* **2002**, *66*, 155211.

(35) Miara, L. J.; Suzuki, N.; Richards, W. D.; Wang, Y.; Kim, J. C.; Ceder, G. Li-ion Conductivity in Li_9S_3N. *J. Mater. Chem. A* **2015**, *3*, 20338−20344.

(36) Miara, L. J.; Richards, W. D.; Wang, Y. E.; Ceder, G. First-principles Studies on Cation Dopants and Electrolyte|cathode Interphases for Lithium Garnets. *Chem. Mater.* **2015**, *27*, 4040−4047.

(37) Mo, Y.; Ong, S. P.; Ceder, G. First Principles Study of the $Li_{10}GeP_2S_{12}$ Lithium Super Ionic Conductor Material. *Chem. Mater.* **2012**, *24*, 15−17.

(38) Nosé, S. A Unified Formulation of the Constant Temperature Molecular Dynamics Methods. *J. Chem. Phys.* **1984**, *81*, 511−519.

(39) Hoover, W. G. Canonical Dynamics: Equilibrium Phase-space Distributions. *Phys. Rev. A: At., Mol., Opt. Phys.* **1985**, *31*, 1695−1697.

(40) Jain, A.; Ong, S. P.; Chen, W.; Medasani, B.; Qu, X.; Kocher, M.; Brafman, M.; Petretto, G.; Rignanses, G.-M.; Hautier, G.; Gunter, D.; Persson, K. A. FireWorks: A Dynamic Workflow System Designed for High-throughput Applications. *Concurrency Computat.: Pract. Exp.* **2015**, *27*, 5037.

(41) Deng, Z.; Radhakrishnan, B.; Ong, S. P. Rational Composition Optimization of the Lithium-Rich $Li_3OCl_{1-x}Br_x$ Anti-Perovskite Superionic Conductors. *Chem. Mater.* **2015**, *27*, 3749−3755.

(42) Jansen, M.; Henseler, U. Synthesis, Structure Determination, and Ionic Conductivity of Sodium Tetrathiophosphate. *J. Solid State Chem.* **1992**, *99*, 110−119.

(43) Wang, Y.; Richards, W. D.; Ong, S. P.; Miara, L. J.; Kim, J. C.; Mo, Y.; Ceder, G. Design Principles for Solid-state Lithium Superionic Conductors. *Nat. Mater.* **2015**, *14*, 1026−1031.

(44) Willems, T. F.; Rycroft, C. H.; Kazi, M.; Meza, J. C.; Haranczyk, M. Algorithms and Tools for High-throughput Geometry-based Analysis of Crystalline Porous Materials. *Microporous Mesoporous Mater.* **2012**, *149*, 134−141.

(45) Martin, R. L.; Smit, B.; Haranczyk, M. Addressing Challenges of Identifying Geometrically Diverse Sets of Crystalline Porous Materials. *J. Chem. Inf. Model.* **2012**, *52*, 308−318.

(46) Murch, G. E. The Haven Ratio in Fast Ionic Conductors. *Solid State Ionics* **1982**, *7*, 177−198.

(47) Morgan, B. J.; Madden, P. A. Relationships between Atomic Diffusion Mechanisms and Ensemble Transport Coefficients in Crystalline Polymorphs. *Phys. Rev. Lett.* **2014**, *112*, 145901.

(48) Bron, P.; Johansson, S.; Zick, K.; Schmedt, J.; Günne, D.; Dehnen, S. S.; Roling, B. $Li_{10}SnP_2S_{12}$: An Affordable Lithium Superionic Conductor. *J. Am. Chem. Soc.* **2013**, *135*, 15694−15697.